Complete Author's reply

Paper Title: Multiscale statistical analysis of coronal solar activity,

by D. Gamborino, D. del-Castillo-Negrete and J.J. Martinell.

Manuscript No.: npg-2015-83

Revised Submission

As requested in the submission website, we group together in this document the detailed responses to the reviews of the two referees, which include each question raised by the referee (written in blue), followed by our response (in black) and afterwards the modification to the text incorporated as a result of the comment if there is one (in red).

First there is the reply to referee #1 and next the reply to referee #2.

This is followed by the new version of the complete manuscript with all the changes made, highlighted in boldface.

We have tried to give a satisfactory answer to all comments. Some of them are incorporated in the new manuscript and some others are discussed with arguments that support our points of view.

We feel the manuscript has improved as a result of the comments and we hope the revised version is appropriate for publication in Nonlinear Proecesses in Geophysics.

Referee #1

We thank the referee for his (her) valuable comments and suggestions. Following is our response and the changes incorporated in the new version of the manuscript. To make the revision more transparent, we have grouped the referee's comments by topics.

Opening paragraph:

Referee's comment:

"This study addresses the spatio-temporal dynamics of the solar corona from a interesting point of view by decomposing coronal temperature maps over a given time interval into small sets of separable modes, similar to what had been pioneered in the 1990s in neutral fluid turbulence by N. Aubry, R. Lima, P. Holmes, G. Berkooz, and more. However, this study looks much like a replication of [Futatani et al., Phys. Plasmas 16, 042506 (2009)] to a solar dataset, without properly taking into account the strong assumptions behind this dataset. In addition, the method is over-interpreted, thus leading to incorrect conclusions"

Authors' response:

We appreciate that the referee finds our approach to the spatio-temporal dynamics of the solar coronal interesting. However we do not agree on the statement that "…this study looks much like a replication of [Futatani, et al. (2009)] ….." The fact that we use the similar data analysis tools does not make our work a replica. In particular, the problem studied in the paper under submission has its own interest since we use actual solar data whereas the problem addressed in [Futatani, et al. (2009)] deals with numerical simulations. We do not agree either with his (her) remarks that the method has been over-interpreted and/or that our conclusions are incorrect. These issues, as well as several others, are addressed below. Having said this, we acknowledge that several parts of our original manuscript needed further explanations and improvements, and we sincerely thank the referee for bringing to our attention points that needed extra work.

General Comments:

Use of temperature maps

Referee's comment:

"Your study heavily relies on the physically appealing concept of coronal temperature. However, the temperature maps as provided by the method of Aschwanden et al. involve several strong assumptions."

Authors' response:

We agree with the referee that the interpretation of the temperature maps provided by the method of Aschwanden involves assumptions that need to be clarified, and we thank him for explicitly pointing this out. Addressing these concerns has improved our manuscript.

However, we want to stress that our analysis of these maps has an intrinsic value independent of the level of justification regarding any given specific physical interpretation of the data. That is, our main contribution is to provide a novel, unique analysis of data that we, as well as the scientific community, believe to be physically meaningful and related to the thermal properties of the solar corona. We assume (hope) that the referee is not implying that the data is meaningless and read his criticism as a valuable call to be more careful regarding the physical interpretation, something we completely agree.

Referee's comment:

"In particular, these temperature maps are assuming an isothermal plasma, which is a coarse approximation of what the true corona is; it certainly does not hold during flaring activity, and it is likely too to be incorrect too during transients, such as your heat fronts."

Authors' response:

We agree with the referee, and have modified the manuscript to explicitly mention the limitations of the interpretation of the data as temperature maps.

Changes incorporated:

Page 5 Line 120 added:

The data we analyze with the methods described in the previous section were obtained from the observations of the Atmospheric Imaging Assembly (AIA) instrument (Boerner et al. , 2012; Lemen et al. , 2012) of the SDO, using the six filters that record the coronal emission. We are interested in the information related to the thermal energy distribution in the corona, which in general is difficult to obtain accurately due to the temperature sensitivity of the emission and radiation transfer processes across the corona. Most of the methods used to obtain temperatures in the solar atmosphere rely on the isothermal assumption. This is a coarse approximation of the solar corona that might not be fully justified in the case of flaring activity. However, following Aschwanden et al. (2013) we adopt this approximation in order to give a simple intuitive physical interpretation of the data.

(4 lines below) Moreover, since we are interested in the thermal energy distribution in the corona and not on the absolute values of the temperature, we only need the relative values of the thermal content and for this we take the "pixel-average" temperature obtained from the method developed by Aschwanden et al. (2013) that was implemented in a SolarSoft routine. From the combination of the six filters dual maps for the emission measure (EM) and temperature are obtained.

(next line) Despite the approximations made, our analysis has an intrinsic value independent of the level of justification regarding any given specific physical interpretation of the data themselves. Our goal is to extract valuable spatio-temporal dependencies given the data that is currently available using the simplest physical assumptions.

Referee's comment:

"In addition, flares cause artifacts such as pixel bleeding. Another good reason to be very careful when interpreting synoptic EUV images."

Authors' response:

We would like to point out that in the data considered in the present work the intensity of the signal is not high enough for the pixel bleeding to be a concern. We are not observing the flare at its peak intensity.

Referee's comment:

"These limitations (which are mentioned in Aschwanden's article) should be considered very seriously before any physical interpretation can be given to these temperature maps. A first and obvious starting point would be to check the width of the temperature distribution, and discard all pixels for which the isothermality assumption does not hold.

Authors' response:

Checking the width of the temperature distribution to discard data for which the isothermal assumption does not hold is a valuable suggestion to post-process the data before analyzing it with the proposed tools. However, this task is outside the scope of the present paper that aims to explore the data directly using the proposed tools using the simplest physical assumptions. Having said this, we have added this valuable suggestion in the manuscript.

Changes incorporated:

Page 5 Line 129 added:

One alternative to avoid potential unintended consequences of the isothermal assumption would be to check the width of the temperature distribution, and discard all pixels for which the assumption does not hold. However implementing this filter is outside the scope of the present manuscript that aims to explore the data directly using the proposed tools.

Referee's comment:

Following this, I'm deeply concerned that the whole interpretation in Sections 3 to 5 remains purely speculative as long as these spurious effects are properly addressed, which may be quite challenging. I would refrain from using temperature maps at all, except for qualitative analysis, or for structures that are known to be approximately isothermal."

Authors' response:

We believe that in our responses to the previous points we have made clear that the data we are using are meaningful; they are based on standard approximations made in the literature. Therefore the analyses made in Sections 3-4 are not speculative but reflect the presence of actual physical processes. Section 5 contains the conclusions and in response to the referee's multiple comments we have, once again, reiterated the role of the approximations involved.

Changes incorporated:

Page 21 Line 392 added:

Using EUV images from six filters of the SDO/AIA and simple physical assumptions (mainly isothermality within a pixel) we have constructed maps representing the energy content 2D distribution that we use as approximate temperature maps for the Solar Corona.

Referee's comment:

"What is then the best observable? Note that most studies consider log(T) rather than T because it is more convenient, and also because the distribution of T is assumed to be log-normal. Several of the properties of the SVD are optimal for datasets that have a normal distribution. For that reason, I would seriously consider working with log(T) rather than with T – assuming of course that the temperature can be used at all."

Authors' response:

It is important to keep in mind that T and log(T) contain exactly the same physical information, and in this sense they are the same observable. Thus, deciding which one is "better" has not an objective answer. In those cases when T is assumed to be log-normal, we agree with the referee that working with log(T) might be more efficient. However, it is important to keep in mind that we are not assuming anything about the statistics of T. In fact, one of the key contributions of this work is to actually compute the PDF of T directly from the data, and to do this accurately we have found that working directly with T has advantages. Having clarified this, we were intrigued by the referee's suggestion and have actually redone the multi-scale decomposition in Figs. 4, 5 and 6 and have observed that they are fundamentally the same for T and log(T) (see figures below as compared to Figs. 4, 5, 6 of the paper) which again confirms the fact that they contain the same information.

Data analysis

Referee's comment:

line 119: why "requires significant emission of radiation" ?

Authors' response:

We do not understand the Referee's question. Line 119 says "significant emission variation" it does not say "significant emission radiation".

Referee's comment:

line 120: what is the time span of your data set, and did you correct for solar rotation ? The latter point is *very* important because the properties of your SVD modes change if your spatial frame is moving.

Authors' response:

The time span of the event analyzed is 80 x 12 sec = 16 min. This is a relatively short time compared to the rotation period of the sun (~27 days). Therefore, there is no need to correct for solar rotation effects.

Changes incorporated:

Page 7 Line 189 added:

For the relatively short duration, solar rotation is unimportant.

Referee's comment:

line 131: For each wavelength there is a corresponding temperature: this is incorrect. Each wavelength is associated with a temperature distribution.

Authors' response:

We agree with the referee and thank him (her) for pointing this out. We have modified the manuscript accordingly.

Changes incorporated:

Page 6 Line 169 added:

Each wavelength is produced by a temperature distribution that peaks at a characteristic temperature, T_{λ}, so the intensity of the line for an emitting region is related to the relative contribution of this temperature.

Referee's comment:

line 134: Do you mean that the filter response is associated with a DEM ?

Authors' response:

No, this is not what was written in the manuscript. However, to avoid potential misunderstanding we have modified the sentence.

Changes incorporated:

Page 6 Line 174:

The physical conditions affecting the radiation are not known in general and are usually represented by the so-called differential emission measure (DEM) which is used to obtain the temperature distribution of the plasma averaged along the line of sight.

Referee's comment:

line 135: note that there are alternate methods for inferring the temperature, such as [Guennou et al., Astrophysical Journal Supplement Series 203 (2012)], and [Dudok de Wit et al., Solar Physics, 283 (2012), pp. 31–47].

Authors' response:

We thank the referee for bringing to our attention these references which we have added to the manuscript.

Changes incorporated:

Page 5 Line 138 added:

Alternate methods for inferring the temperature have also been developed by Guennou et al. (2012) and Dudok de Wit et al. (2013).

Referee's comment:

line 158: why that particular size of 32x32 ? Why not larger or smaller ? What is limiting the number of time steps ? Notice that since Nx*Nx » Nt, in your covariance matrix your ensemble average is done along the spatial dimension, and not along the more usual temporal one. This impacts your results, and should be addressed.

Authors' response:

The pixel number was determined by the size of the region where the moving front was present during the chosen time span which turned out to be 32X32. The number of time frames was limited by the selection criteria mentioned in section 3. We are not doing any ensemble average, our method follows the standard procedure of unfolding the space data in a vector to form the space-time matrix.

Indeed there is a larger number of space points Nx*Ny that time points Nt but there is no problem with this. The results we show do not involve any ensemble average.

Changes incorporated:

Page 8 Line 202 added:

The length traveled by the thermal front set the size of all the regions analyzed, included the pre-flare and quiet sun cases, so they can be compared directly.

Referee’s comment:

Fig. 4: what are there oblique stripes in all of your pictures, as if the plasma was moving sideways ? Since your spatial region is a square, it would make more sense to force its aspect ratio to 1.

Authors’ response:

Because these stripes show up in the topos diagrams they are not related to propagation events. Most likely they are due to a spatial correlation at the corresponding scale. The referee is right about the aspect ratio equals 1, we are changing it in the new version.

Changes incorporated:

Page 9 and 10, modified aspect ratio in Figures 4, 5 and 6.

Referee’s comment:

line 175: why plot the absolute value ? and how should it better reveal periodicities ?

Authors’ response:

We were looking for a correlation between periods of activity and the mode rank so the only information needed is the amplitude of $v^k(t\_j)$. However, since no correlation was found we decided that there is no need to mention that and therefore we have removed this comment from the new version.

SVD analysis

Referee’s comment:

“I also have major concerns regarding your interpretation of the SVD results. In line 178, you say that "there is some correlation between small scales and high frequencies". This is merely a consequence of the properties of the SVD, and has nothing to do with the physics. Whenever you diagonalise a covariance matrix (what the SVD does, in some way) whose values decay monotonically as you move away from the diagonal, then the eigenmodes (your topos and chronos) will be like Fourier modes whose number of nodes will increase with the rank k. So, small wavenumbers will automatically be associated with small frequencies.

Authors’ response:

In the SVD the relevant scales for each rank come out as a result of the analysis. Therefore, although in a given problem wavenumbers and frequencies might increase with increasing rank they don't necessarily might do it uniformly or at the same rate. Thus, any potential correlation between spatio-temporal scales cannot be a priori assumed and needs to be unveiled using the SVD. In fact, in the SVD analysis of the solar data, such correlation is not found in the pre-flare or quiet sun regions as seen in Fig. 8. An even more dramatic example is the analysis presented in [Futatani et. al. (2009)] (See Figs. 8, 11, 13 and 15 of that paper) where the correlation between the spatial and temporal scales for different ranks was shown to depend fundamentally on the intrinsic physical properties of the underlying turbulence. It is easy to construct examples of surrogate data sets that contradict the referee statement that this “is merely a consequence of the properties of the SVD, and has nothing to do with the physics”. Consider for instance, a dataset generated from the function $f(x,y,t)=\sum_{j=1}^{N} A_j \cos(k_j(x+y))\cos(\omega_j t)$ which represents the superposition of pure modes with associated amplitudes A_j that determine the energy content of each mode. Depending on how A_j, k_j and ω_j are ordered the SVD would produce different correlations between space and time scales. To illustrate the point we constructed two datasets with just 10 modes (N=10) with amplitudes in decreasing order $A_j=(20,18,16,..,4,2,0.1)$; SVD will then order the modes according to *j*. When the wave numbers and frequencies are both monotonically decreasing $k_j, \omega_j=(10,\ldots,1)$ one expects a direct correlation between time and space scales. When we apply the same processing used in the paper to this data, the plot obtained for the scales τ and λ is shown in the next figure on the LHS. On the other hand, when the frequencies increase monotonically $\omega=(1,\ldots10)$ keeping k_i decreasing, there should be an inverse correlation, and this is indeed what is found as shown on the RHS of the figure. That shows that the relation between space and time scales is not merely a consequence of the SVD analysis but comes as a results of intrinsic properties of the data.

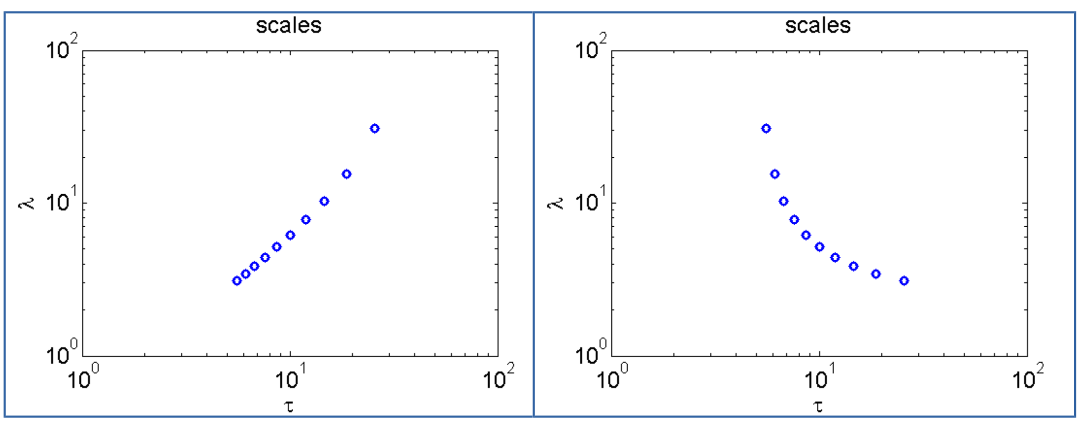

In the new version we limit to pointing out the different degrees of correlation for the three cases studied, but we do not mention any relationship with cascading, as indicated below.

Referee’s comment:

Try to generate a surrogate dataset that has the same second order properties, and you'll get exactly the same results. For that same reason, there is no evidence whatsoever for a cascading (line 193). Incidentally, because the SVD exploits second order moments only, I would not recommend in problems in which phase coherence matters."

Referee's comment:

line 193: see general comments. There is no cascading whatsoever here.

Authors' response:

It is not clear what the referee means by second order properties or phase coherence. As explained below eq. 5 our use of SVD is based on finding the best approximation of data based on the Frobenius norm. This minimization process takes into account the whole spatial temporal dependence of the dataset. Having said this we agree that the interpretations of a cascading process are too preliminary at this point and needs further investigation. Accordingly we decided to remove this and address this interesting issue in a future publication.

Referee's comment:

"Later on (line 195) you introduce the scaling index gamma: this makes no sense because several of your topos and chronos don't have a clear characteristic size, or time scale. You may find values for <kappa> and <f>, but this does not prove that they make sense as they would, for example, for a wavelet basis."

Authors' response:

We do not agree with the referee's statement that "topos and chronos do not have characteristic size" since the modes shown in the diagrams have an associated scale seen as the size of the small granulations in the topos part and a dominant frequency in the chronos part. Given this fact the Fourier modes do provide the characteristic scales.

Even though the correlation of spatio-temporal scales may not be interpreted as a cascade, the type of correlation does have some information that can be extracted when such a correlation exists. It conveys information about how the energy content in each rank is distributed in time and space scales. In other works it has been found to be diffusive-like (gamma=1/2) or super-diffusive (gamma>1/2) (Futatani et al. 2009). When no correlations can be found (as in pre-flare and quiet sun cases) a fitting cannot be found and nothing can be concluded for those cases.

Referee's comment:

"Several more details suggest that you're over-interpreting what the SVD is telling. I strongly recommend that you check your results carefully and test them, in particular by using surrogate data. This also applies to Figure 9, from which one cannot draw serious conclusions without knowing what the confidence intervals of the singular values and energy spectra are."

Authors' response:

Figure 9 contains the information on how the method captured the amplitude of the different modes, and it is important to determine the relative weight of them. The analysis is based in a single space-time dataset folded into a matrix and there are no statistical variations that would require the assesment of a confidence interval.

Referee's comment:

"your title is misleading as you are not truly doing a multiscale analysis. The SVD does indeed separate different scales, but these are very loosely defined, and are in no way comparable to what truly multi-resolution techniques, such as the wavelet decomposition, would give."

Authors' response:

SVD and wavelets are both multi-scale analysis tools that depending on what you want to study. Each one has advantages and disadvantages; see for example Futatani et al. (2011).

The scale decomposition in the SVD is based on the energy content which is a well defined mathematical concept. One advantage of SVD is that it does not specify the mode structure a priori but it is determined as a result of the analysis. In that sense we feel the title is not misleading.

Referee's comment:

"the POD is strictly identical to the SVD, not more general"

Authors' response:

Not quite, in fact the SVD is a general mathematical technique used to factorize matrices that has been applied to many different problems beyond mode decomposition. In our context of data analysis, POD and SVD are indeed the same. To avoid controversies, we have removed any statement implying there is any difference between them.

Changes incorporated:

Page 2 Line 26 added:

This method (SVD) is equivalent to the proper orthogonal decomposition (POD) that has been applied in many contexts …

Referee's comment:

"many more studies have used the SVD, or variants thereof to investigate the spatio-temporal dynamics of the Sun. I would be good to mention some of them, and not focus only on the work by Vecchio et al."

Referee's comment:

“line 33: topos and chronos are not a method, but just the names given to the spatial, resp. temporal modes obtained by applying the SVD to a spatiotemporal dataset, see [N. Aubry et al., Journal of Statistical Physics, 64 (1991), pp. 683–739]. BTW, in that context, the SVD is called biorthogonal decomposition.”

Referee’s comment:

“line 33 the specific method: all these methods (POD, biorthogonal decomposition, SVD, EOF, PCA ...) are identical; what distinguishes them to some degree is the type of data they are applied to, or the preprocessing, but even that is not always true. So there is no point mentioning them as if they were different. Otherwise people keep on reinventing the wheel.”

Referee’s comments:

“line 88: mention at least the original work by Aubry, Lima, et al, who coined the words topos and chronos.”

line 208: T should also be indexed by t_i

Fig. 10: please use symbols that can be read on B/W printouts.

Authors’ response:

We agree with these comments, so we have modified the text accordingly in the right places.

Changes incorporated:

Page 2 Line 33 added:

The implementation of the method that incorporates time and space variations, was referred to as Topos-Chronos by Aubry el al. (1991) and has been used in several studies to perform spatio-temporal analyses of turbulence (Benkadda et al. , 1994; Futatani et al. , 2011), and of some solar features (Carbone et al. , 2002; Mininni et al. , 2002, 2004; Lawrence et al. , 2005; Podladchikova, et al. , 2002; Vecchio et al. , 2009) under different names. Here we apply it to study the space-time evolution of different solar coronal regions.

Referee’s comment:

“line 94: unfolding –> folding end of 2.1: again, what is the physical motivation behind working with A^{(r)} ?”

Authors’ response:

“Unfolding” is correct because we mean converting an array of rows (matrix) to a single long row (vector) (one matrix row after the other). The motivation of working with

$A^{(r)}$ has been included.

Referee’s comment:

For example, for the rank 1 mode you capture the average background temperature, whose spatial or temporal scale is of no particular interest here, should definitely be excluded from your analysis.

Referee’s comment:

line 199: the mode with rank 1 is just the average background. Usually, when analyzing a spatio-temporal wavefield that is quasi-stationary (as is the case here, as T stays around 10^6 C), that first mode should be discarded since it doesn’t tell us much about the dynamics. What matters is the variation on top of it.

Referee’s comment:

line 210: for the reason explained just above, since you’re interested by the dynamics only, you should start by subtracting the time-average from each pixel. This will affect the distribution of the singular values. The wording "energy" will then make much more sense as it truly describes the variance of the modes.

Authors’ response:

The rank 1 mode has important information too, including time dependence; that is why we keep it. In fact the analysis on heat transport of Section 4.2 is mostly based on this mode. Subtracting the rank 1 would be misleading. The analysis mentioned by the referee would provide different information.

Front and solar flares

Referee’s comment:

“what is it you are calling a heat front ? Flares are intense events that generate various types of transients. So-called EIT waves have received considerable attention [Gallagher and Long, Space Science Reviews, 158 (2011), pp. 365–396] but they’re not the only ones. Here, I strongly recommend that you put your analysis in context, and emphasize the novelty of your results in comparison to existing studies.”

Author's response:

What we call a heat front is simply an emitting thermal structure that moves across the solar disk. The actual identification of the structure with any of the waves found in the solar atmosphere (EIT, Moreton waves, etc) is not important to us. However, a short discussion about the possible comparison with these waves has been included.

Changes incorporated:

Page 5 Line 146:

What we call a heat front is simply an emitting thermal structure that moves across the solar disk, but we are not interested in the actual identification of it with known waves in the solar atmosphere. There could be various possibilities for the propagating front such as EIT waves (Gallagher and Long , 2011), coronal waves related to chromospheric Moreton 145 waves (Narukage et al. , 2004) or others, which are known to perturb some structures like in the wave-filament interactions (Liu el al. , 2013). It is, however, not relevant to our studies to know which type of perturbation is seen.

Referee's comment:

line 35: why is flaring activity interesting ? section 2.1 this part is clearly written, but quite mathematical, and devoid of a connection with the physics. It would help to say the your spatio-temporal wakefield gets decomposed into a finite series of separable modes of time and space, which, in addition, are orthonormal, etc.

Authors' response:

Section 2.1 gives a short introduction to the basics of SVD; but we added the physical connection and the short description suggested by the referee.

Changes incorporated:

Page 3 Line 68:

In our case, SVD is used to decompose spatio-temporal data into a finite series of separable modes of time and space, which are orthonormal. The modes give the best representation of the relevant time and space scales of the data.

Referee #2

We thank the referee for his (her) valuable comments and suggestions. Following is our response and the changes incorporated in the new version of the manuscript.

Referee's comment

SUMMARY AND GENERAL EVALUATION

The authors present an interesting spatio-temporal analysis of 4-dim solar data, for a flaring event, the preflare phase, and a Quiet Sun region. They use a Singular Value Decomposition method and investigate the multi-scale behavior of the physical parameter of the temperature T, and attempt to extract information on the heat flow dT/dx in a flare. The description of the method is clear, and the data analysis steps are described in sufficient detail. In the second half of the paper the authors try to extract information on the heat flux before and during a flare, where they arrive at the result that diffusive transport is not relevant in solar flares, which is at odds with other studies. If the authors can reconcile the interpretation of this controversial result in terms of the limitations of the used method, the paper may possibly be suitable for publication.

Authors' response:

We do not really say that diffusion is not relevant in solar flares in general, we say that, for the particular event analyzed, transport is dominated by advection. However, we only considered transport along the main direction of propagation of the heat front (*x*). Prompted by the referee's comments, we extended the analysis to the propagation in the perpendicular direction (*y*), where advection is not expected to play an important role, in order to capture the diffusive contribution. As a result, we have found a correlation between the heat flux, q_y and grad T would allow, in principle, to estimate a diffusion coefficient. This additional results are included in the present version of the manuscript; we do not mention anymore that diffusion is not observed. Only for transport along *x* it is subdominant.

Changes incorporated:

Page 18: The formulation for transport along *y* was added with boldface font, starting with line 343 and Figure 15 was incorporated to illustrate the results.

Page 18 Line 332 added:

In contrast, the negative temperature gradient has no clear correlation with Q(x) which seems to indicate that diffusion is not the main drive for the heat flux along *x in this particular event*.

DETAILED COMMENTS

Referee's comment:

In the Discussion and Conclusions the authors arrive at several important and some controversial results:

(1) "... a raw correlation between Fourier time scale and spatial scales during the flare,

but not for pre-flare or quiet Sun. This may indicate that the flare-driven heat flows tend to decay into smaller scales, in a cascade-like process." - Perhaps a reference and discussion can be made whether this is relevant to the scenario of "inverse MHD turbulent cascade" (e.g., Abramenko et al. 2003, ARep 47, 151, "Pre-Flare Changes in the Turbulence Regime for the Photospheric Magnetic Field in a Solar Active Region"; Antonucci et al. 1996, ApJ 456, 833 " Interpretation of the observed plasma turbulent velocities as a result of magnetic reconnection in solar flares"; LaRosa,T.N. and Moore,R.L. 1993, ApJ 418, 912-918, "A mechanism for bulk energization in the impulsive phase of solar flares: MHD turbulent cascade".

Authors' response:

We appreciate the referee's suggestion. It would certainly be interesting to do this discussion to enrich the paper. However, we have not included this because we decided to remove the interpretation of a cascading process, since, as pointed out by the other referee, this conclusion seems to be premature in the light of our results. We will take it into account for a future work on this subject.

Referee's comment:

(2) "... The pre-flare activity seems to produce larger low-amplitude fluctuations, characteristic of intermittency, which might herald the occurrence of the flare." — Discuss in this in the context of the paper by Abramenko et al. (2003), for instance.

Authors' response:

We thank the referee for the suggestion and we completely agree with its pertinence. We have included this discussion in the new version of the manuscript.

Changes incorporated:

Page 23 Line 412 added:
It is interesting to note that this result may be related to the findings of Abramenko et al. (2003) who also showed that there is evidence of intermittency in the magnetic field of an active region previous to the occurrence of a flare. They argue that this indicates that there is a turbulent phase before the flare, which would be in agreement with the intermittency in the temperature fluctuations found here.

Referee's comment:

(3) "A multi-scale analysis of the heat flux was also performed for the region associated with the flare. The thermal flux profiles along the main direction (x) of the flow were computed using original temperature maps and compared with the temperature variation along x, allowing to obtain the advection velocity profile. Diffusive transport is found to be not relevant." — This is contrary to other observational findings that the envelope of the flare area propagates like diffusive transport (Aschwanden 2012, ApJ 757, 94, "The spatio-temporal evolution of solar flares observed with AIA/SDO: Fractal diffusion, sub-diffusion, or logistic growth". The author’s result may be biased because

they use a 1-dim transport model (in x-direction), with no transport in transverse direction.

Authors' response:

We are actually not implying that there is no diffusive transport. What we find is that, *in this case*, transport is dominated by convection because of the strong heat pulse. However, as explained above, the analysis of transport along *y* direction has modified this assertion. As pointed out by the referee, the 1D model produces a bias but this was offset by the addition of the transport in the perpendicular direction. Diffusive processes are much weaker than advection for transport along the direction of propagation of the heat front, but it is noticeable for transport in the perpendicular direction. We have commented this issue in the new version.

Changes incorporated:

Page 23 Line 420 added:

Diffusive transport is found to be sub-dominant and cannot be evaluated. A similar analysis was performed for transport along the direction perpendicular to the heat front propagation and in that case diffusion shows as an important contribution to transport.

Page 23 Line 428 added:

We point out that indications about a diffusive-like transport associated with a solar flare have been found by Aschwanden (2012) who actually found that the transport is sub-diffusive. This agrees with our result of Fig.7 which shows that the correlation of time and space scales corresponds with a sub-diffusive process.

Referee's comment:

Furthermore, they assume that there is no energy source inside the region of temperature maps (line 270). It would be more realistic to assume that the energy transport is isotropic in all directions, because the high-resolution images from AIA show that a flare entails many reconnection sites with magnetic field lines that go in all directions. Perhaps the authors can modify their heat flux model accordingly, or at least discuss the limitations of their model and what bias is expected in the diagnostics of the overall heat flux from a (point-like) flare source region.

Authors' response:

We are actually analyzing a small region very close to the brightest flaring region but that does not include it (see Fig. 3). The heat front moves away from the main flare site as it advances and penetrates into the region of study. The flare is not assumed to be point-like but rather it is outside our control volume. Therefore, it is valid to assume there are no energy sources inside the volume; most reconnection sites are in the flaring region which is outside. On the other hand, we cannot assume that transport is isotropic because of the strong contribution of advection which is directed along a specific direction in the case we study. But this issue is addressed by the modifications adding transport along *y*, as mentioned above. We have included a mention to the need of extending the model.

Changes incorporated:

Page 18 Line 343 added:

However, diffusive transport can be noticeable in the y direction where an important advection is not present. This can be studied with a similar analysis by averaging across the x direction. Notice that the averaging procedure is a simplification that would produce only approximate results.

Manuscript prepared for Nonlin. Processes Geophys.
with version 2014/09/16 7.15 Copernicus papers of the LaTeX class copernicus.cls.
Date: 28 April 2016

Multiscale statistical analysis of coronal solar activity

Diana Gamborino[1], Diego del-Castillo-Negrete[2], and Julio J. Martinell[1]

[1]Instituto de Ciencias Nucleares, UNAM,, A. Postal 70-543, México D.F., Mexico
[2]Oak Ridge National Laboratory,, Oak Ridge, TN, 37831, USA

Correspondence to: J.J. Martinell (martinel@nucleares.unam.mx)

Abstract. Multi-filter images from the solar corona are used to obtain temperature maps which are analyzed using techniques based on proper orthogonal decomposition (POD) in order to extract dynamical and structural information at various scales. Exploring active regions before and after a solar flare and comparing them with quiet regions we show that the multiscale behavior presents distinct statistical properties for each case that can be used to characterize the level of activity in a region. Information about the nature of heat transport is also to be extracted from the analysis.

1 Introduction

The increasing number of space telescopes and space probes that provide information about phenomena occurring in the space is yielding enormous amount of data that need to be analyzed to get information about the physical processes taking place. In particular, images of the Sun obtained from the Solar Dynamics Observatory (SDO) instruments and the new Interface Region Imaging Spectrograph (IRIS) mission have a remarkable high resolution that allow studies of the Sun with great detail, not available before. The analysis of the images usually involves some processing if one has to extract information not readily obtained from the raw images. Some techniques used for image analysis and feature recognition in the Sun have been described by Aschwanden (2010). A useful tool that gives information about the physical conditions in the emitting region is the emission measure (EM) which is obtained from images in several wavelengths; this in turn provides the local temperature of the emitting region (e.g., Aschwanden and Boerner , 2011). When the EM is computed for all the pixels in a given region of the Sun, the temperature maps can be obtained. There are some computational tools developed in SolarSoftWare (SSW) that take images from different instruments at the available filters to produce EM and temperature maps (e.g. for Yohkoh, SOHO, TRACE, SDO).

The images can be processed for pattern recognition using techniques such as wavelet analysis that sort the structures in terms of the scaling properties of their size distribution (Farge and Schneider , 2015). Another method, which is also frequently used in image compression, is the singular value decomposition (SVD) of the pixel matrix. This method **is equivalent to the proper orthogonal decomposition (POD) that** has been applied in many contexts including: *solar physics* (Vecchio et al. , 2005, 2008) *image processing* (Rosenfeld and Kak , 1982); and *turbulence models* (Holmes et al. , 1996). Applications to plasma physics relevant to the present work include compression of Magnetohydrodynamics data del-Castillo-Negrete et al. (2007); detection of coherent structures (Futatani et al. , 2009), and multi-scale analysis of plasma turbulence (Futatani et al. , 2011; Hatch et al. , 2011). In this work we apply POD techniques to a time sequence of images representing temperature maps of the solar corona. The **implementation of the method that incorporates time and space variations, was referred to as Topos-Chronos by Aubry el al. (1991) and has been used in several studies to perform spatio-temporal analyses of turbulence (Benkadda et al. , 1994; Futatani et al. , 2011), and of some solar features (Carbone et al. , 2002; Mininni et al. , 2002, 2004; Lawrence et al. , 2005; Podladchikova, et al. , 2002; Vecchio et al. , 2009) under different names. Here we apply it to study the space-time evolution of different solar coronal regions.** The analysis of solar flare activity is of particular interest as it is the more energetic phenomena in the Sun linked with structural changes that may be detected with this method. To this end we perform an analysis of temperature maps corresponding to a region of solar flare activity, and compare the results with the analysis done in the *same* region *before* the solar flare and in a “quiet" region where no flares were detected during the time of observation. Our POD multi-scale study is supplemented with a statistical analysis of the probability distribution function (PDF) of temperature fluctuations. In particular, in the search for statistical precursors of solar flare activity, we show that the small scale temperature fluctuations in pre-flare states exhibit broader variability (compared to the flare and quiet sun states) and the corresponding PDFs exhibit non-Gaussian, stretched-exponential tails characteristic of intermittency. We also present a study heat transport during solar flare activity based on a simplified analysis that allows to infer the transport coefficients (advection velocity and diffusivity profiles) from the data.

The rest of the paper is organized as follows. In section 2 the fundamentals of POD methods are presented and the features of the Topos-Chronos method as the optimal representation of a truncated matrix are explained. Section 3 describes how the data for temperature maps are obtained for a solar flare event and for other solar regions. The results of applying the POD methods to the data are described in section 4 highlighting the statistical features of the multi-scale analysis. This leads to the identification of intermittency in an active region previous to a flare. As a further application, section 4.2 presents the evaluation of heat transport coefficients based on the full temperature maps and on POD. Finally, in section 5 we give the conclusions of the analysis and an appraisal of the POD methods applied to solar physics.

2 Description of POD methods used in the work.

In this section we review the basic ideas of the POD method and its application in separating spatial and temporal information as used in the present work.

2.1 SVD

The Singular Value Decomposition (SVD) is, generally speaking, a mathematical method based on matrix algebra that allows to construct a basis in which the data is optimally represented. It is a powerful tool because it helps extract dominant features and coherent structures that might be hidden in the data by identifying and sorting the dimensions along which the data exhibits greater variation. **In our case, SVD is used to decompose spatio-temporal data into a finite series of separable modes of time and space, which are orthonormal. The modes give the best representation of the relevant time and space scales of the data.**

The SVD of the matrix $A \in \mathbb{R}^{m\times n}$ is a factorization of the form,

$$\mathbf{A} = \mathbf{U}\Sigma\mathbf{V}^T \tag{1}$$

where $U \in \mathbb{R}^{m\times m}$ and $V \in \mathbb{R}^{n\times n}$ are orthogonal matrices (i.e. $U^TU = VV^T = I$) and $\Sigma \in \mathbb{R}^{m\times n}$ is a rectangular diagonal matrix with positive diagonal entries. The N diagonal entries of Σ are usually denoted by σ_i for $i = 1, \cdots, N$, where $N = \min\{m,n\}$ and σ_i are called singular values of A. The singular values are the square roots of the non-zero eigenvalues of both AA^T and A^TA, and they satisfy the property $\sigma_1 \geq \sigma_2 \geq \cdots \geq \sigma_N$.(Golub and van Loan , 1996; Martin and Porter , 2012)

Another useful mathematical expression of SVD is through the tensor product. The SVD of a matrix can be seen as an ordered and weighted sum of rank-1 separable matrices. By this we mean that the matrix A can be written as the external tensor product of two vectors: $u \otimes v$ or by its components: $u_j v_k$, i.e.,

$$A = \sum_{i}^{r} \sigma_i u_i \otimes v_i^T \tag{2}$$

where $r = \mathrm{rank}(A)$. Here u_i and v_i are the i-th columns of U and V respectively. Equation (2) is convenient when one wants to approximate A using a matrix of lower rank. In particular, according to the Eckart-Young Theorem (Eckart and Young , 1936), given eq. 1, the truncated matrix of rank $k < r = \mathrm{rank}(A)$

$$A^{(k)} = \sum_{i=1}^{k} \sigma_i u_i \otimes v_i^T. \tag{3}$$

is the optimal approximation of A in the sense that

$$\| A - A^{(k)} \|^2 = \min_{\mathrm{rank}(B)=k} \| A - B \|^2$$

over all matrices B, where $\parallel A \parallel = \sqrt{\sum_{i,j} A_{ij}^2}$ is the Frobenius norm.

In our analysis the matrix $A(x,y)$ is the scalar field representing the temperature **or the energy content** at each point x, y at a given time. **Thus, we have a time sequence of** maps that are represented by the 2D spatial rectangular grid (x_i, y_j) where $i = 1, \ldots, N_x$ and $j = 1, \ldots, N_y$. The maximum number of elements in the SVD expansion (eq. (3)) is, therefore, $k = \min\{N_x, N_y\}$. These maps change as a function of time.

2.2 Topos and Chronos

Topos and Chronos is **a name given to the the separation of time and space variations in the data in a way that the POD method can be applied** (Aubry el al. , 1991; Benkadda et al. , 1994). To illustrate this technique, consider a spatio-temporal scalar field $A(\boldsymbol{r}, t)$ representing the temperature T, where $\boldsymbol{r} = (x, y)$. We introduce a spatial grid (x_i, y_j) with $i = 1, \ldots, n_x$ and $j = 1, \ldots, n_y$ and discretize the time interval $t \in (t_{in}, t_f)$, as t_k with $k = 1, \ldots, n_t$, $t_1 = t_{in}$ and $t_{n_t} = t_f$. We represent the data as a 3D array $A_{ijk} = A(x_i, y_j, t_k)$. Since the SVD analysis applies to 2D matrices, the first step is to represent the 3D array as a 2D matrix. This can be achieved by "unfolding" the bf rows of the 2D matrix of the spatial domain of the data into a single row 1D vector, i. e. $(x_i, y_j) \to \boldsymbol{r}_i$ with $i = 1, \ldots, n_x \times n_y$, and representing the spatio-temporal data as the $(n_x n_y) \times n_t$ matrix $A_{ij} = A(r_i, t_j)$, with $i = 1, \ldots, n_x \times n_y$ and $j = 1, \ldots, n_t$.

The singular value decomposition of $A(r_i, t_j)$ is given by the tensor product expression,

$$A_{ij} = \sum_{k=1}^{N^*} \sigma_k u_k(r_i) v_k(t_j), \tag{4}$$

where $N^* = min[(n_x n_y, n_t)]$. In this sense, the POD represents the data as a superposition of separable space time modes.The vectors u_k and v_k satisfy the orthonormality condition given by,

$$\sum_{i=1}^{n_x n_y} u_k(r_i) u_l(r_i) = \sum_{j=1}^{n_t} v_k(t_j) v_l(t_j) = \delta_{kl}. \tag{5}$$

The $n_x n_y$-dimensional modes u_k are the "topos" modes, because they contain the spatial information of the data set, and the n_t-dimensional modes v_k are the "chronos" since they contain the temporal information.

From eq. (3), we define the rank-r optimal truncation of the data set A^r as,

$$A_{ij}^{(r)} = \sum_{k=1}^{r} \sigma_k u_k(r_i) v_k(t_j). \tag{6}$$

where $1 \leq r \leq N^*$. The matrix $A^{(r)}$ is the best representation of the data due to the fact that, by construction, the POD expansion minimizes the approximation error, $\parallel A - A^r \parallel^2$.

3 Temperature data maps.

The data we analyze with the methods of previous section are obtained from the observations of the Atmospheric Imaging Assembly (AIA) instrument (Boerner et al. , 2012; Lemen et al. , 2012) of the SDO, using the six filters that record the coronal emission. We are interested in the information related to the thermal energy distribution in the corona, which in general is difficult to obtain accurately due to the temperature sensitivity of the emission and radiation transfer processes across the corona. Most of the methods used to obtain temperatures in the solar atmosphere rely on the isothermal assumption. This is a coarse approximation of the solar corona that might not be fully justified in the case of flaring activity. However, following Aschwanden et al. (2013) we adopt this approximation in order to give a simple intuitive physical interpretation of the data. One alternative to avoid potential unintended consequences of the isothermal assumption would be to check the width of the temperature distribution, and discard all pixels for which the assumption does not hold. However implementing this filter is outside the scope of the present manuscript that aims to explore the data directly using the proposed tools. Moreover, since we are interested in the thermal energy distribution in the corona and not on the absolute values of the temperature, we only need the relative values of the thermal content and for this we take the "pixel-average" temperature obtained from the method developed by Aschwanden et al. (2013) that was implemented in a SolarSoft routine. From the combination of the six filters dual maps for the emission measure (EM) and temperature are obtained. Alternate methods for inferring the temperature have also been developed by Guennou et al. (2012) and Dudok de Wit et al. (2013). Despite the approximations made, our analysis has an intrinsic value independent of the level of justification regarding any given specific physical interpretation of the data themselves. Our goal is to extract valuable spatio-temporal dependencies given the data that is currently available using the simplest physical assumptions.

The first step is to select appropriate events that contain the phenomenology of interest. In our case, we focus on the propagation of a heat front associated with an impulsive release of energy, such as a solar flare. **What we call a heat front is simply an emitting thermal structure that moves across the solar disk, but we are not interested in the actual identification of it with known waves in the solar atmosphere. There could be various possibilities for the propagating front such as EIT waves (Gallagher and Long , 2011), coronal waves related to chromospheric Moreton waves (Narukage et al. , 2004) or others, which are known to perturb some structures like in the wave-filament interactions (Liu el al. , 2013). It is, however, not relevant to our studies to know which type of perturbation is seen.** We look for events satisfying the following criteria: (1) Flares of medium intensity (classification C according to Geostationary Operational Environmental Satellite (GOES)) for which no saturation of the image occurs. (2) Significant **contrast of the flare related structures emission, in order to have a clear identification. This selects active-region**

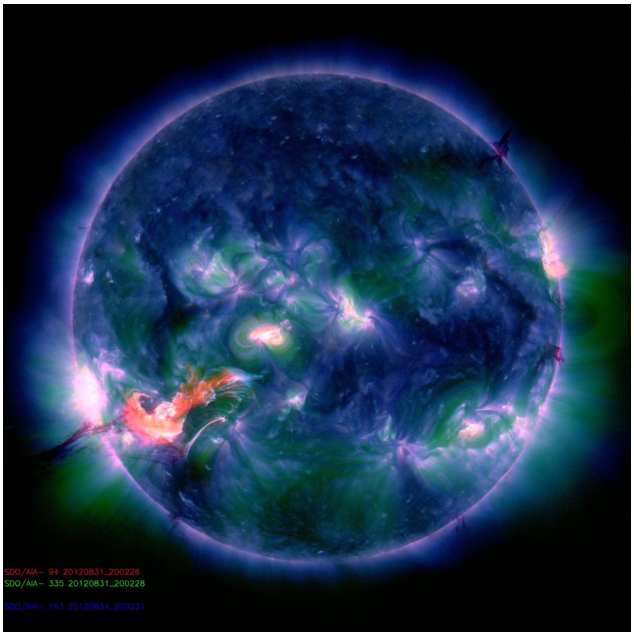

Figure 1. AIA Composite of EUV emissions (94, 193, 335 Å) [Ref.: http://sdo.gsfc.nasa.gov].

events which are also compared to the same active region before the event and to a quiet sun region at the same period.

The chosen event occurred on 31/8/2012 at around 20:00 UT. There were seven active regions on the visible solar disk. An image at a fixed time is shown in Fig. 1, formed from a compound of extreme ultraviolet (EUV) emissions (94,193, 335 Å) from the solar corona. Active region 11562 was the originator of the solar flare of GOES-class C8.4.

The AIA instrument consists of four detectors with a resolution of 4096×4096 pixels, where the pixel size corresponds to a space scale of $\approx 0.6''$ (≈ 420 km). It also contains ten different wavelengths channels, three of them in white light and UV, and seven in EUV, whereof six wavelengths (131, 171, 193, 211, 335, 94 Å) are centered on strong iron lines (Fe VIII, IX, XII, XIV, XVI, XVIII), covering the coronal range from $T \approx 0.6$ MK to $\gtrsim$ 16MK. AIA records a full set of near-simultaneous images in each temperature filter with a fixed cadence of 12 seconds. More detailed instrument descriptions can be found in Lemen et al. (2012) and Boerner et al. (2012).

Each wavelength is produced by a temperature distribution that peaks at a characteristic temperature (T_λ), so the intensity of the line for an emitting region is related to the relative contribution of this temperature. Thus, the images of the different intensities, $F_\lambda(x, y)$, can be used to obtain maps of the coronal temperature. These intensities represent the measured photon flux, which is determined by **the emission process, the physical conditions in the region traversed by the photons** and the filter response. **The physical conditions affecting the radiation are not**

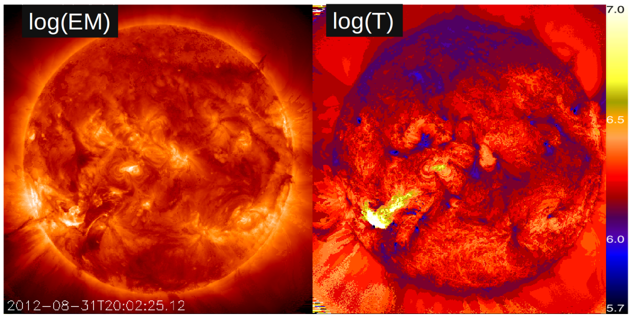

Figure 2. Emission Measure map (left) and Temperature map (right).

known in general and are usually represented by the so-called *differential emission measure* (DEM) which is used to obtain the temperature distribution of the plasma averaged along the line of sight.

The DEM distribution $[dEM/dT]$ is typically given by $dEM(T) = n^2 dh/dT$ [cm^{-5} K^{-1}], where $n(h(T))$ is the electron density at height h and with temperature T. The DEM distribution DEM= $d[EM(T,x,y,z)]/dT$ can be reconstructed from the six filter fluxes $[F_\lambda(x,y)]$, and in (Aschwanden et al. , 2013) developed a method to compute the peak emission measure (EM) and the peak temperature T_p for each pixel based on a simple representation of the DEM by a Gaussian function of temperature, for each filter. Then, model fluxes are computed from the expression

$$F_\lambda(x,y) = \int DEM(T,x,y) R_\lambda dT$$

where $R_\lambda(T)$ are the filter response functions at a given wavelength, which are fitted to the observed flux $F_\lambda^{obs}(x,y)$. This determines the best-fit values for EM and T_p thus obtaining the temperature maps. Here we use the Automated Emission Measure and Temperature map routines developed by Aschwanden et al. (2013) that implement the method of multi-Gaussian functions based on six-filter data, following a forward-fitting technique. The result of applying this post-processing methodology on the data in Fig. 1 is shown in Fig. 2. **Notice that the colors show values of log(T). Due to the uncertainties mentioned above, these maps are not true temperature maps but they provide information about the energy content distribution in the 2D space, and we can call them temperature-like maps**. The "temperature´´ map covers a temperature interval in the range $\log(T) = 5.7 - 7.0$ shown in the vertical bar. It highlights the hot regions while the EM map is more sensitive to the plasma density, since it is proportional to the square of the electron density (independent of temperature). Temperature maps were computed for a time span of 16.4 minutes with a cadence of 12 seconds, as provided by the AIA data. In total, 82 maps were generated. **For the relatively short duration, solar rotation is unimportant.**

4 Results of the analysis

The **maps** generated in the previous section combining the emission at six wavelengths can be further processed to extract structures and dynamical features **related to the thermal energy content**. The time evolution of the data space array, $A(x,y,t)$, is analyzed with the POD method described in Section 2. We first focus on the heat front that propagates from left to right in the region close to the flare site. From these maps we can extract information concerning: (1) the nature of the heat transport and (2) the physical conditions in the region. In particular, we seek to obtain information from the analysis about the energy distribution in the different spatial scales and how this compares with other regions with no flares. Fig. 3 presents the region where a heat front is moving at selected times in the full time interval; the vertical lines indicate the position of the leading-front at the initial and final times. We limit the attention to this region which is a square with dimensions $N_x \times N_y$ with $N_x = N_y = 32$ pixels (in these maps one pixel is 2.4" $\times$ 2.4"). **The length traveled by the thermal front set the size of all the regions analyzed, included the pre-flare and quiet sun cases, so they can be compared directly.** The POD method can be applied in a systematic way to separate time and space features and study them with a multi-scale analysis, or to determine the underlying features of heat transport.

The same POD analysis performed on the temperature maps in Fig. 3 is also applied to two other temperature maps corresponding to (a) exactly the same physical region but about one hour before the appearance of the flare (to which we refer as *pre-flare*) and (b) a different region in the quiet sun for the same time interval as the first map (referred to as *quiet-sun* or QS). These other analyses are made in order to compare the properties of the three cases and be able to determine the features associated with flare activity in the solar corona.

4.1 Multiscale statistical analysis using Topos-Chronos decomposition

As mentioned in subsection 2.2, the POD represents the data as a superposition of separable space-time modes. Figures 4, 5 and 6 show the result of applying this process to the three cases mentioned: after Solar flare, Pre-flare and Quiet Sun, respectively. The figures include behavior for small ranks, $k = 1,2,3,4$ and large ranks, $k = 20,30,40,46$. The 2D plots in the first and third columns present the spatial distribution, topos modes $u_k(r_i)$, rescaled by the singular values σ^k. The second and fourth columns show the chronos POD modes $v^k(t_j)$. One can see from Fig. 4 for the flare time, that, **as expected,** low-k chronos modes exhibit a low frequency variation while large-k modes exhibit high frequency burst activity. A similar behavior is found for the topos modes in which large scale structures are seen for low k while a granulated structure with small scales is found for high k. **Although this is a natural consequence of the Topos-Chronos decomposition, it is of interest to determine the degree of correlation between space scales and time scales as the rank k changes**.

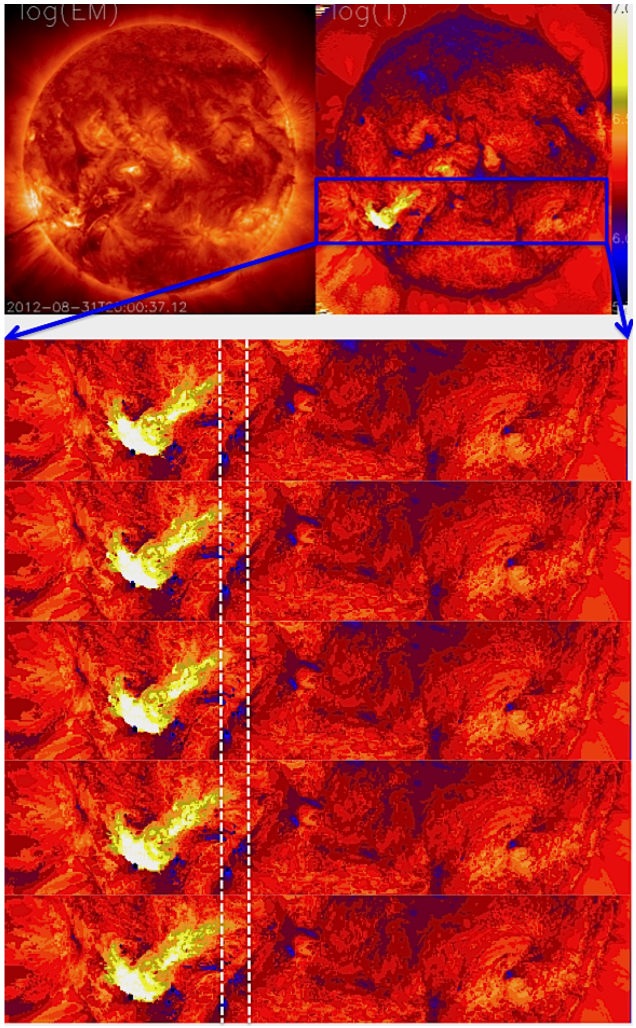

Figure 3. Snapshots at different times of the region where the heat front is moving.

225 This correlation can be studied using Fourier analysis to extract the characteristic spatiotemporal scales of each POD mode. For the Topos modes, we first transform the one-dimensional vector r_i back to space coordinates x_l and y_m and compute the two-dimensional Fourier transform, $\hat{u}_k(\kappa_{x_l}, \kappa_{y_m})$. The characteristic length scale of the topos rank-k mode is then defined as the mean length scale of the corresponding Fourier spectrum, $\lambda(k) = 1/\langle \kappa_k \rangle$, where $\langle \kappa_k \rangle$ is defined as:

230 $$\langle \kappa_k \rangle = \frac{\Sigma_{i,j} |\hat{u}_k(\kappa_{xi}, \kappa_{yj})|^2 (\kappa_{xi}^2 + \kappa_{yj}^2)^{1/2}}{\Sigma_{i,j} |\hat{u}_k(\kappa_{xi}, \kappa_{yj})|^2} \tag{7}$$

Using the same procedure, we associate a characteristic time scale τ to each chronos $v_k(t_m)$ mode using $\tau(k) = 1/\langle f_k \rangle$ with:

$$\langle f_k \rangle = \frac{\Sigma_m |\hat{v}_k(f_m)|^2 f_m}{\Sigma_m |\hat{v}_k(f_m)|^2} \tag{8}$$

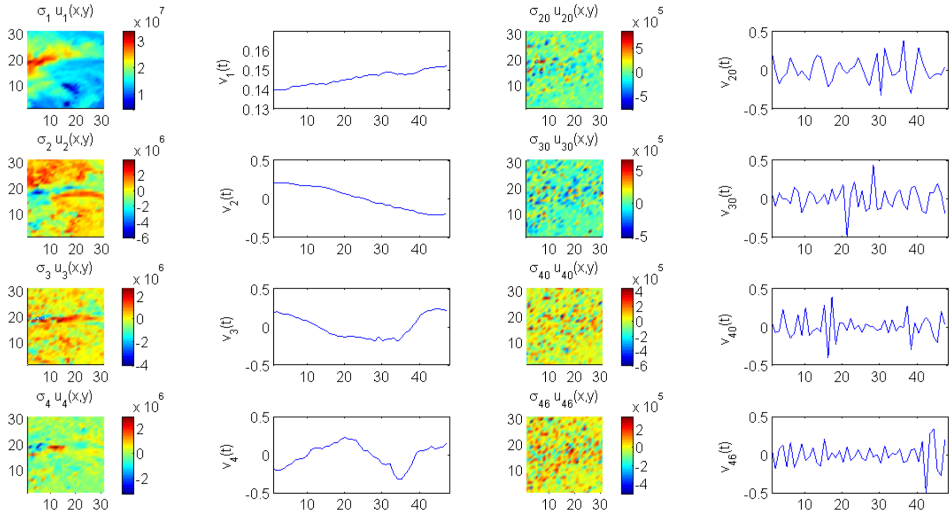

Figure 4. Topos-Chronos decomposition of solar flare activity. Odd columns: spatial modes $u_k(r_i)$; even columns: temporal modes $v_k(t_j)$, for k=1,2,3,4,20,30,40,46. One unit in the time axis equals 12 s.

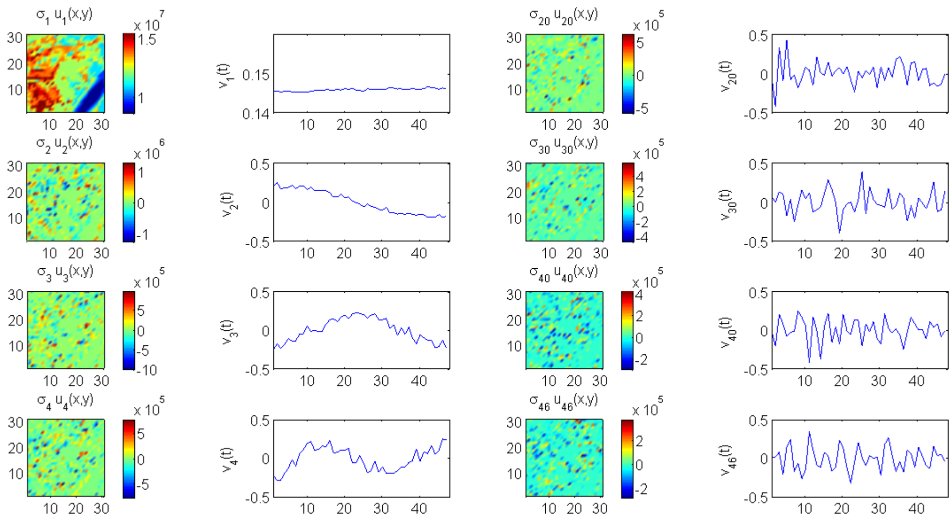

Figure 5. Topos-Chronos decomposition of pre-flare solar activity. Odd columns: spatial modes $u_k(r_i)$; even columns: temporal modes $v_k(t_j)$, for k=1,2,3,4,20,30,40,46. One unit in the time axis equals 12 s.

where $\hat{v}_k(f_m)$ is the Fourier transform in time of $v_k(t_m)$. Figure 7 shows the characteristic length scale $\lambda(k)$ versus the characteristic time scale $\tau(k)$ for all ranks. The tendency for increasing time scale with increasing space scales is apparent, although there is some dispersion for small space-time scales. The scaling can be fitted by a power law of the type $\lambda \sim \tau^{\gamma}$ and in this case $\gamma = 0.11$. For

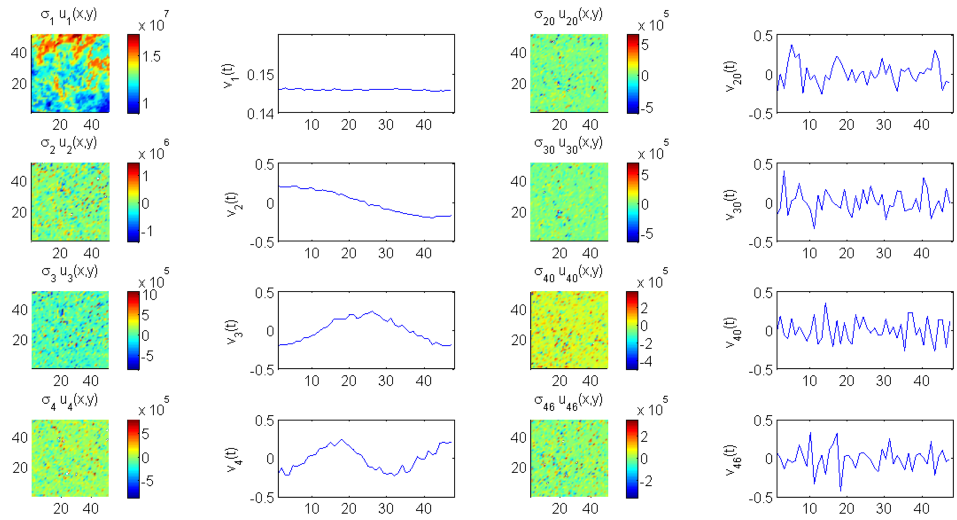

Figure 6. Topos Chronos decomposition of quiet sun region. Odd columns: spatial modes $u_k(r_i)$; even columns: temporal modes $v_k(t_j)$, for k=1,2,3,4,20,30,40,46. One unit in the time axis equals 12 s.

a diffusive-like process $\gamma = 1/2$, thus this results suggests that a sub-diffusive heat transfer may be taking place.

The topos-chronos plots for the pre-flare and quiet-sun cases in Figs. 5 and 6 do not show a clear correlation of the time and space scales. One can notice that only for rank 1 there are dominant large spatial scales while for higher ranks there are only small scales present. In the chronos diagrams the dominant small frequencies seen at low k have higher frequency oscillations superimposed. In order to determine if there is any correlation between spatio-temporal scales we make the same Fourier analysis as for the case with flare. The resulting length and time scales for all ranks are shown in Figure 8 for the two regions, pre-flare and QS. It is clear that for these cases no correlation is found and thus, it is not possible to attribute any cascading-like process, as in the region affected by the flare.

Further information can be obtained from the reconstruction error in the POD representation, defined as the difference $\delta T_{t_i}^{(r)} = T_{t_i} - T_{t_i}^{(r)}$ where T is the original temperature map at a given time t_i, and $T_{t_i}^{(r)}$ is the reconstructed map up to rank-r at the same time t_i. Since a measure of the total energy content in the data is given by $E = \sum_{ij} A_{ij}^2 = \sum_{k=1}^{N^*} \sigma_k^2$, the energy contained in the reconstruction to rank-r is

$$E(r) = \sum_{k=1}^{r} \sigma_k^2$$

with σ_k^2 giving the partial energy contribution of the kth-mode. Thus, the reconstruction error $|\delta T_{t_i}^{(r)}|^2$ contains the remaining energy in the leftover ranks $E - E(r)$. In particular, for high r, $\delta T_{t_i}^{(r)}$ is as-

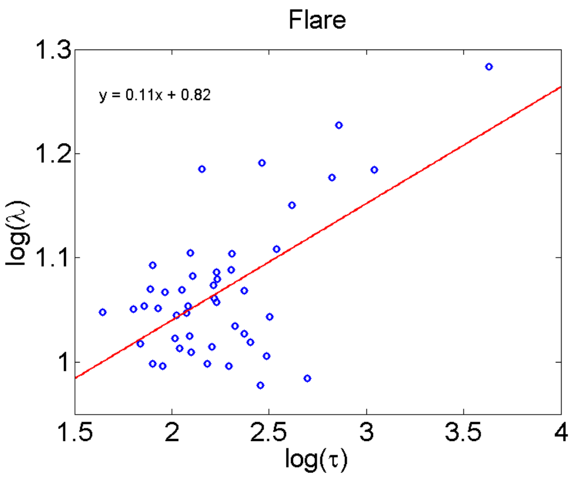

Figure 7. Length scale vs time scale for all POD ranks; Solar flare.

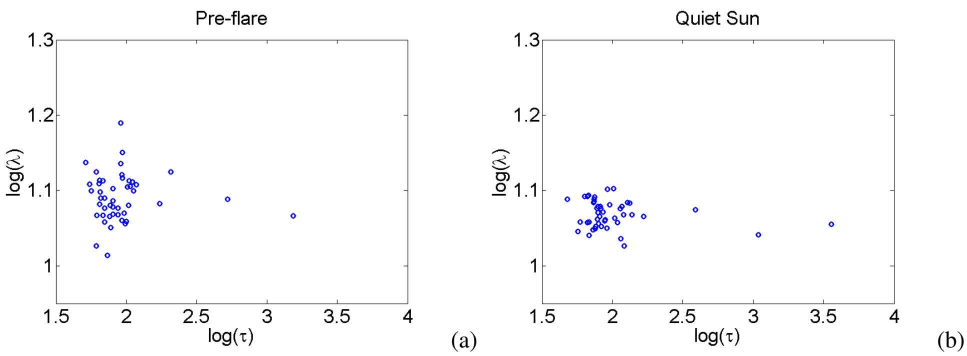

Figure 8. Length scale vs time scale for all POD ranks: (a) Pre-flare and (b) Quiet Sun.

sociated with the energy in the small scales. Given that the singular values, satisfying $\sigma_k \leq \sigma_{k+1}$, decay very fast in the first few modes, as seen in the POD spectra of Figure 9(a) for the three cases analyzed, most of the energy is contained in the low-r reconstructions. To see this, Figure 9(b) shows the energy contribution percentage, $E(r)/E$, as a function of the reconstruction rank-r for the three cases under study. It is clear that the first mode already contains about two thirds of the energy and successive modes contribute less as the rank rises. The case with the flare has the energy distributed over more modes, reflecting the effect of the large scale flows produced by the flare.

To quantify the degree of the temperature intermittency, we construct the probability distribution function (PDF) by dividing the range of values of $T - T_{t_i}^{(r)}$ in small bins and counting the number of grid points of the map falling in each bin. The resulting histogram represents the PDF of $T - T_{t_i}^{(r)}$ and this can be done for different percentages of the energy contribution, i.e. taking the corresponding rank r from Fig. 9(b). We chose to use two energy fractions to compare them, namely a residual energy of 10% and 25% (i.e. $1 - E(r)/E$). For each case, there is one PDF for each time t_i having its own height and width, but we expect them to have similar statistical features. Thus, as it is customary,

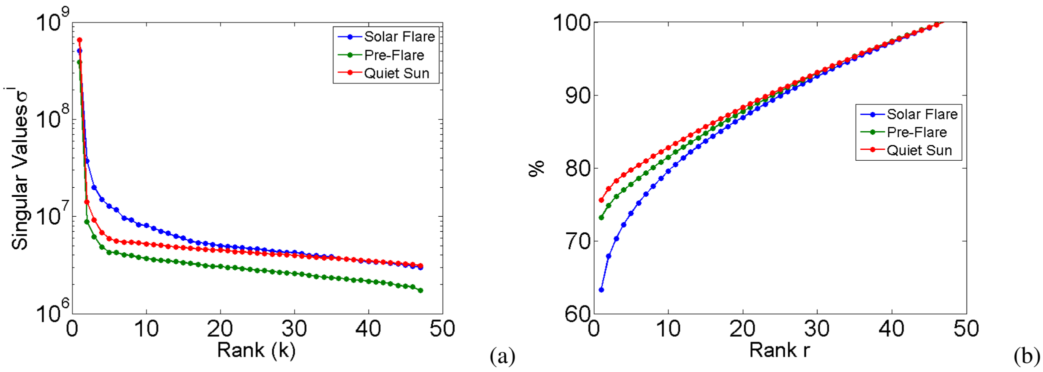

Figure 9. (a) Singular values spectra σ^k as a function of k. (b) Energy contribution percentage of the rank-r reconstruction.

we rescale the PDF as $P \to \sigma P$ and $x \to x/\sigma$ where σ is the standard deviation. Since σ changes with the different time frames, it is more convenient to use the average $\langle\sigma\rangle_t$ over all times in order to have a single normalizing parameter. Thus, for every time the PDFs were rescaled with the average standard deviation as $P \to \langle\sigma\rangle_t P$ and $\delta T^r_{t_i} \to \delta T^r_{t_i}/\langle\sigma\rangle_t$. It is found that the resulting rescaled PDFs are all quite similar having a small overall dispersion. Then we took the average over the time sequence of PDFs (47 frames) in order to have a single PDF that represents the statistical properties of the reconstruction error maps for each energy content. The results for the two energy percentages are shown in figure 10. It is observed that the PDFs of the pre-flare region are significantly broader than the other two, indicating the presence of very large temperature fluctuations.

In order to determine if the PDFs have non standard features like long tails, it is useful to fit some known function to the data. Normal statistics produce a Gaussian PDF, so we can fit a stretched exponential $P(x) \sim \exp(-\beta|x|^{\mu})$ to the average PDFs in order to asses how far they are from a Gaussian ($\mu = 2$). In Figure 11 we show the best fits to each of the six cases analyzed. For each PDF we present a fit of the central part and another fit of the tails (with smaller μ). Clear differences are observed among the Flare, Pre-flare and QS cases. However, for the different energy contents, the results do not show great variability. The interesting result is that pre-flare PDFs, in addition to being the broadest of the three (see Fig. 10), have the lowest values of μ and so they are the ones that depart the most from a Gaussian; the long tails indicate there is intermittency, i.e. a relatively large number of intense temperature fluctuations. On the other hand, the PDFs for the Flare have larger μ and thus are closer to a Gaussian; large fluctuation events are then less frequent. Our results agree with the study in Futatani et al. (2009) that observed lower levels of intermittency in the presence of sources. The work in Futatani et al. (2009) followed the transport of impurities in a plasma with decaying turbulence (without sources to sustain it) finding evidence of intermittency, but it disappears when there are sources that maintain the turbulence. In our case, the flare plays the role of a source that

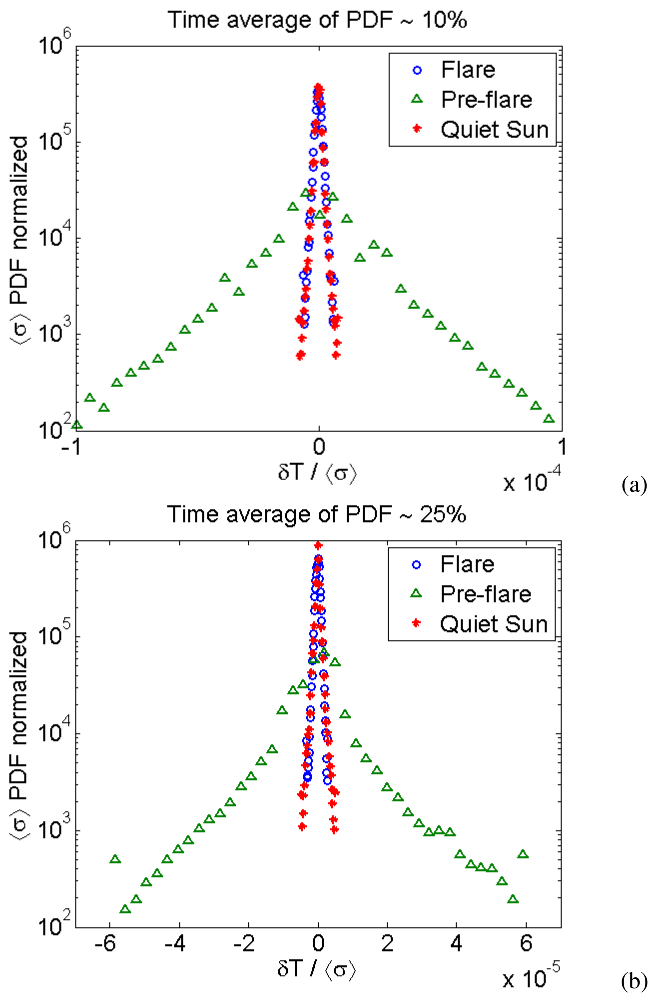

Figure 10. PDF averaged over time frames for energy content in the small scales of (a) 10 % (more reconstruction modes) and (b) 25 % (less reconstruction modes)

suppresses intermittency. As expected for a region with no solar activity, in the quiet sun case, the PDF does not exhibit long tails, i.e., the probability of large temperature fluctuations is small.

4.2 Heat Flux Estimate

In this section we focus on the region affected by the flare and calculate the thermal flux entering there, driven by the released flare energy. This is made using the time evolution of the original temperature maps and comparing the results with those obtained with the Topos-Chronos method. Next, the heat flux is used to explore the properties of heat transport in the corona.

Since the thermal front produced by the flare is a coherent structure it is expected that the main mechanism bringing energy into the region of interest is advective. Using this premise, we use the computed heat flux to estimate the velocity of the incoming plasma flow, as a function of the coor-

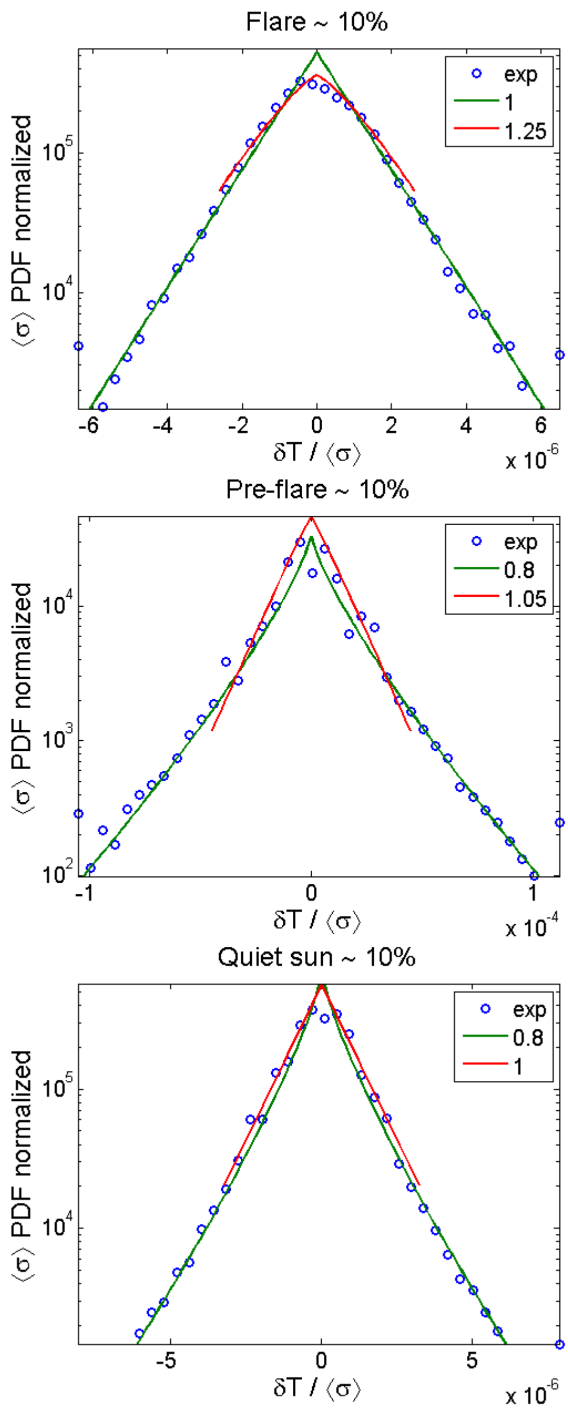

Figure 11. Stretched exponential fits of the temperature fluctuations PDFs when energy content in small scales is 10 %; μ values are given in the legends. (a) Flare [$\mu = 1, \beta = 9.75 \times 10^5$ and $\mu = 1.25, \beta = 1.82 \times 10^7$], (b) Pre-flare [$\mu = 0.8, \beta = 9 \times 10^3$ and $\mu = 1.05, \beta = 1.3 \times 10^5$] and (c) Quiet Sun [$\mu = 0.8, \beta = 9.1 \times 10^4$ and $\mu = 1, \beta = 10^5$].

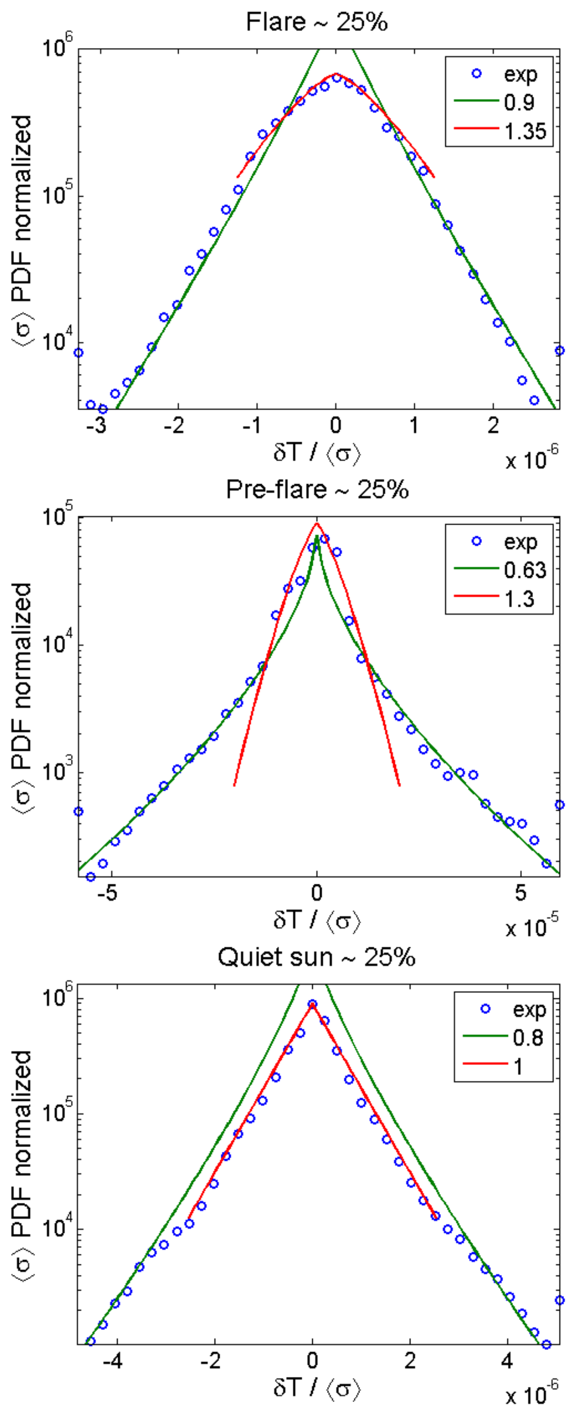

Figure 12. Stretched exponential fits of the temperature fluctuations PDFs when energy content in small scales is 25 %; μ values are given in the legends. (a) Flare [$\mu = 0.9, \beta = 6.3 \times 10^5$ and $\mu = 1.35, \beta = 9 \times 10^4$], (b) Pre-flare [$\mu = 0.63, \beta = 2.8 \times 10^3$ and $\mu = 1.3, \beta = 1.5 \times 10^8$] and (c) Quiet Sun [$\mu = 0.8, \beta = 1.5 \times 10^5$ and $\mu = 1, \beta = 1.7 \times 10^6$].

dinate x along the flow (the velocity profile $V(x)$). However, there might be a diffusive component playing part in the process. To investigate this, we compare the heat flux profile with the temperature and temperature gradient profiles to look for convection or diffusion relations. Assuming that both processes coexist, we estimate velocity profiles taking different levels of diffusion. We also explore the scenario of diffusion being the main transport process by computing the profiles of the diffusivity $D = D(x)$, but we find that it is not viable since D becomes negative.

For the analysis of the heat flux we make the following assumptions: (1) there are no sources of energy inside the region of the temperature maps since it was chosen to be slightly away from the flare site; (2) the main direction of motion is along the x-axis (y displacements are negligible and no information of the dynamics in the z-axis is known: we have an integrated view along z); (3) the internal energy of the plasma is $u = \frac{3}{2} n k_B T$ and no mechanical work is done by the plasma; (4) we use a constant electron density with the value for the lower solar Corona: $n = 10^{15}$ m^{-3} in the region of interest.

Total Heat Flux using Original T-maps: The starting point is the heat transport equation in the absence of sources:

$$\frac{3}{2} n k_B \frac{\partial T}{\partial t} = -\nabla \cdot \boldsymbol{q} \tag{9}$$

Since the thermal front moves almost exclusively in the x direction, we assume that the y variations are not very relevant and therefore we take the average of eq. (9) over y. Moreover, we are interested in the energy transport over the whole time interval, τ, and therefore we take the time average of eq.(9)

$$\frac{3}{2} n k_B \left\langle \overline{\frac{\partial T}{\partial t}} \right\rangle_y = -\langle \overline{\nabla \cdot \boldsymbol{q}} \rangle_y \tag{10}$$

where $\langle f \rangle_y = \frac{1}{L} \int_0^L f dy$ is the average value in the y-direction and $\overline{f} = \frac{1}{\tau} \int_0^\tau f dt$ is the time average. Integrating eq.(10) along the x-coordinate and using that there is no flux through the upper and lower egdes, i.e. $\langle \partial q_y / \partial y \rangle_y = 0$, we get:

$$\begin{aligned} \frac{3}{2} n k_B \int_x^L \left\langle \overline{\frac{\partial T}{\partial t}} \right\rangle_y (x') dx' &= \int_x^L \frac{\partial}{\partial x'} \langle \overline{q_x} \rangle_y dx' \\ &= \langle \overline{q_x} \rangle_y (L) - \langle \overline{q_x} \rangle_y (x) \end{aligned}$$

Assuming that the first term on the right hand side is zero, meaning there is no heat leaving the region at $x = L$, the average heat flux profile is

$$\langle \overline{q_x} \rangle_y (x) = \frac{3}{2} n k_B \int_x^L \langle \Delta_\tau T \rangle_y dx'. \tag{11}$$

where $\Delta_\tau \xi \equiv (\xi(t = \tau) - \xi(t = 0))/\tau$.

In Figure 13 we show the heat flux profile computed from the original temperature maps using (11), **for the averaged 1D model**. The heat flux can have an advective and a diffusive component

$\mathbf{Q} = W\mathbf{v} - D\nabla W$ (we do not consider here radiative transport) with $W = nk_BT$ the thermal energy density and D the heat diffusivity. The relative importance of these contributions can be assessed by computing the profiles for the temperature and the temperature gradient and comparing them with the heat flux profile. The temperature profile is taken by averaging the original temperature maps in t and y and similarly for the temperature gradient. These are also shown in Fig. 13 which indicates that the $T(x)$ profile is similar to the $Q(x)$ profile suggesting that the advective component should be the dominant one. In contrast, the negative temperature gradient has no clear correlation with $Q(x)$ which seems to indicate that diffusion is not the main drive for the heat flux **along** x ***in this particular event***. From these observations we can compute the advection velocity as

$$v = \frac{Q + Dnk_B\nabla T}{nk_BT}$$

In Figure 14 the velocity profile computed in this way is shown for the case with no diffusion ($D = 0$) and when a constant diffusivity is assumed to be present ($D_0 = (5\ \text{ and } 15) \times 10^{10} m^2 s^{-1}$). Diffusivities larger than $1.5 \times 10^{11} m^2 s^{-1}$ will give sign changes in v which is unlikely to occur in a heat front, **so this value sets an upper limit to D. This limit is consistent with the values found with other methods which are in the range $10^2 - 10^4 km^2/s$ (Aschwanden , 2012).** We could also explore the possibility of detecting diffusive transport by computing the diffusivity, $D = (v - Q/nk_BT)T/\nabla T$. **When this is done it is found that D has negative values at several points along x which indicates that diffusive transport in the x direction is subdominant**. There can only be a small contribution superimposed on the advective transport. **However, diffusive transport can be noticeable in the y direction where an important advection is not present. This can be studied with a similar analysis by averaging acrosss the x direction. Notice that the averaging procedure is a simplification that would produce only approximate results. The equivalent of Eq. 11 is**

$$\langle \overline{q_y} \rangle_x (y) = \frac{3}{2} nk_B \left[\langle \Delta_\tau T \rangle_{xy}\, y - \int_0^y \langle \Delta_\tau T \rangle_x \, dy'. \right] \tag{12}$$

where it was used again that $\overline{q_y}$ vanishes at $y = 0, L$ and $\langle . \rangle_{xy}$ is the double average over x and y. Eq. 11 was used to express $\overline{q_x}$ at $x = 0$. Using these estimates, Figure 15 shows the averaged heat flux profile across y, together with averaged temperature and temperature gradient profiles. In this case, no correlation can be observed between $\overline{q_y}$ and the temperature and thus the advection is not a dominant process as it was for the flux along x. The temperature gradient has large fluctuations due to the averages in x and time of a widely varying temperature distribution. However, there is some consistency with the heat flux, like the vanishing values of both at the edges and a rough correlation near the central part of the region. Therefore, we can assert that diffusion is probably the dominant process in the y direction. A diffusion coefficient cannot be estimated because of the weak correlation resulting from our approximation. The order of magnitude obtained for the region where there is a correlation turns out to be too

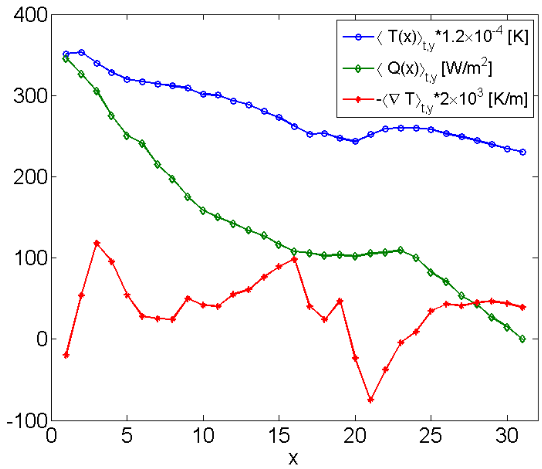

Figure 13. Averaged (in t and y) profiles calculated from the original full temperature maps, for temperature (Blue); heat flux (Green); and negative temperature gradient (Red).

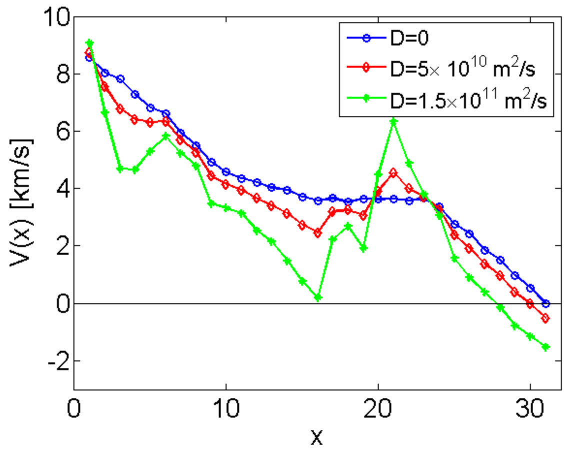

Figure 14. Velocity profiles assuming different levels of constant diffusivity.

large, of order $10^{11} m^2/s$. But since advection is not a candidate, diffusive transport is then an acceptable model for propagation perpendicular to the heat front direction.

Heat Flux using Topos-Chronos:

In addition to the decomposition of the temperature fluctuations in optimal modes, the Topos-Chronos method can be used to do a multi-scale analysis of transport. The separation of space and time allows the extraction of prominent spatial structures persistent over the time span, ordered by rank. Similarly, temporal representation gives information about the time evolution of the structures

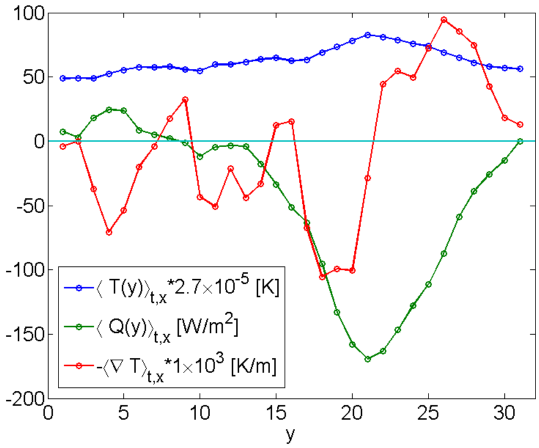

Figure 15. Averaged (in t and x) profiles calculated from the original full temperature maps, for temperature (Blue); heat flux (Green); and negative temperature gradient (Red)..

at the corresponding rank. This separation is amenable to compute the dominant spatial temperature gradients, that drive the heat fluxes, and the time variation of the thermal energy, independently.

Substituting the representation for the temperature maps in eq. 4 into eq.(11) we obtain the Topos-Chronos decomposition of the heat flux profile **along x**:

$$\sum_{k=1}^{N^*} \langle \overline{q_x} \rangle_y (x) = \frac{3}{2} n k_B \int_x^L \left\langle \Delta_\tau \sum_{k=1}^{N^*} \sigma^k u^k(r_i') v^k(t_j) \sigma^k \right\rangle_y dx'$$

The time derivative as well as the time average affect only the temporal modes; the integral and the average in y affect only the spatial modes. When the space components $u^k(r_i)$ are transformed back to a 2D array using the coordinate transformation $r_i \to (x_l, y_m)$, we obtain the matrix $\hat{u}^k(x_l, y_m)$. Each mode of the heat flux is thus given by

$$\langle \overline{q_x} \rangle_y^k (x) = \frac{3}{2} n k_B \sigma^k \Delta_\tau v^k \int_x^L \left\langle \hat{u}^k(x', y) \right\rangle_y dx'. \tag{13}$$

The heat flux profiles for the first four modes are shown in Figure 16. As expected, the dominant mode $k = 1$ has a profile similar to that of the raw temperature maps in Fig. 13. For the other ranks the flux is smaller but, interestingly, for $k = 2$, Q is negative, indicating there is a second order return heat flow.

A similar analysis can be made for the $k = 1$ mode. The result is presented in Figure 17 where, as before, a correlation between $Q(x)$ and $T(x)$ is observed, but not between $Q(x)$ and the temperature gradient. Thus, it is again concluded that advection is the dominant mechanism and the advection velocity can be computed in the same way. The resulting velocity profile is shown in Figure 18 together with the velocity obtained from the original maps for comparison. The Topos-Chronos velocity is larger in most of the region because it lacks the contributions from higher modes, especially the

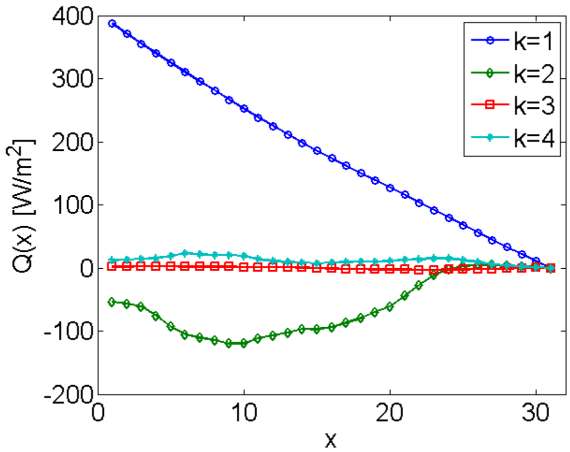

Figure 16. Heat flux profiles as a function of x for four values of the rank k.

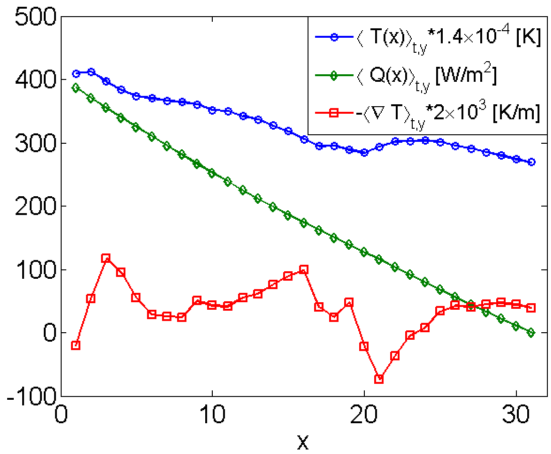

Figure 17. Averaged (in t and y) profiles calculated using Topos-Chronos for rank *k=1*, for temperature (Blue); heat flux (Green); and negative temperature gradient (Red).

negative $k = 2$ rank. **But notably, this shows that for the first mode the heat front has a uniform deceleration all along the path; higher modes are responsible for the small variations. While the $k = 1$ mode has not the complete information, it reveals the presence of some underlying uniform transport porcess.** Higher modes could also provide information about the small scale diffusive transport. However, a quantitative analysis to estimate the diffusivity cannot be done since, as before, it turns out to give negative values at some points. This is because taking the average over the y direction is not a good procedure for this purpose since the contribution of small scales is washed out and this is important for higher modes. The same statement holds for transport along y averaged over x.

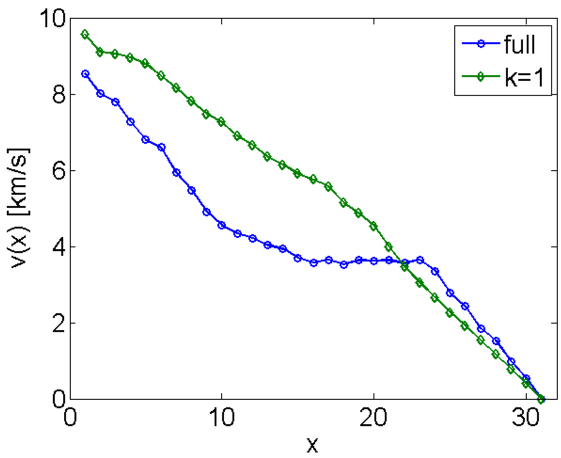

Figure 18. Velocity profiles assuming different levels of constant diffusivity.

5 Discussion and Conclusions

Using EUV images from six filters of the SDO/AIA and simple physical assumptions (mainly isothermality within a pixel) we have constructed maps representing the energy content 2D distribution that we use as approximate temperature maps for the Solar Corona. The temperature maps for a solar event near an AR in the Solar Corona were analyzed using POD methods and were compared with similar analyses of other maps: one of the same region but before the flare (pre-flare) and another of a quiet region during the same time period (quiet sun). The POD method separates time and space information (Topos-Chronos) thus allowing to determine the dominant space-time scales. The high-rank modes in the decomposition correspond to smaller spatial scales and in some degree with small time-scales. An interesting finding is that there is a rough correlation between Fourier time and spatial scales when the flare has occurred but not for pre-flare or QS states. This may indicate that flare-driven large scale heat flows tend to transfer their energy to smaller scales.

The Topos-Chronos method was also used to study the statistical properties of the temperature fluctuations. In particular, we reconstructed the temperature maps up to a certain rank, associated with a given energy content. The reconstruction error was thus associated with the small-scale temperature fluctuations. The probability distribution functions (PDFs) of these small-scale fluctuations were obtained for all times and then averaged in time for each of the three regions analyzed. One of the main results of the present paper is the observation that the PDF for the pre-flare state is significantly broader and has longer tails than the PDFs of the flare and quiet sun cases. The pre-flare activity seems to produce more high-amplitude temperature fluctuations, characteristic of intermittency, which might herald the occurrence of the flare. **It is interesting to note that this result may be related to the findings of Abramenko et al. (2003) who also showed that there is evidence of intermittency in the magnetic field of an active region previous to the occurrence of a flare.**

They argue that this indicates that there is a turbulent phase before the flare, which would be in agreement with the intermittency in the temperature fluctuations found here.

A multi-scale analysis of the heat flux was also performed for the region associated with the flare. The thermal flux profiles along the main (x) direction of the flow were computed using the original temperature maps and compared with the temperature variation along x, allowing to obtain the advection velocity profile. Diffusive transport is found to be **sub-dominant and cannot be evaluated. A similar analysis was performed for transport along the direction perpendicular to the heat front propagation and in that case diffusion shows as a considerable contribution to transport.** The same computations were applied for the Topos-Chronos decomposition finding also a prevalence of advection with a $v(x)$ profile for the lowest mode that agrees with the one for the original maps **and suggesting the presence of an underlying uniform transport process**. Higher modes are not so relevant for the advective flux but can provide information about small scale diffusion. **We point out that indications about a diffusive-like transport associated with a solar flare have been found by Aschwanden (2012) who actually found that the transport is sub-diffusive. This agrees with our result of Fig.7 which shows that the correlation of time and space scales corresponds with a sub-diffusive process.**

Acknowledgements. We thank Dr. Alejandro Lara for his assistance with the use of SolarSoft and IDL. We acknowledge the use of a SolarSoft pachage developed by M. Aschwanden to obtain temperature maps. This work was partially supported by DGAPA-UNAM IN109115 and CONACyT 152905 Projects. D dCN acknowledges support from the Oak Ridge National Laboratory, managed by UT-Battelle, LLC, for the U.S. Department of Energy under contract DE-AC05-00OR22725.

References

Abramenko, V.I., Yurchyshyn, V.B., Wang, H., Spirok, T. J., Goode, P. R.: Signature of an avalanche in solar flares as mesaured by photospheric magnetic fields, Astrophys. J., 597, 1135-1144, 2003.

Aschwanden, M. J.: Image processing techiniques and feature recognition in solar physics, Solar Phys., 262, 235-275, 2010. doi:10.1007/s11207-009-9474-y.

Aschwanden, M. J.: The spatio-temporal evolution of solar flares observed with aia/sdo: fractal diffusion, sub-diffusion, or logistic growth?, Ap. J., 757, 94-115, doi:10.1088/0004-637X/757/1/94, 2012.

Aschwanden, M. J., Boerner, P.: Solar corona loop studies with the atmospheric imaging assembly. I. cross-sectional temperature structure, Ap. J., 732, 81, doi:10.1088/0004-637X/732/2/81, 2011.

Aschwanden, M. J., Boerner, P., Schrijver, C. J., Malanushenko, A.: Automated Temperature and Emission Measure Analysis of Coronal Loops and Active Regions Observed with the AIA on the SDO, Solar Phys., 283, 5-30, 2013.

Aubry, N., Guyonnet, R., Lima, R.: Spatiotemporal analysis of complex signals: Theory and applications, J. Stat. Phys., 64, 683-739, 1991.

Boerner, P., Edwards, C., Lemen, J., Rausch, A., Schrijver, C., Shine, R., Shing, L., Stern, R., Tarbell, T., Title, A., Wolfson, C.J.: Initial Calibration of the Atmospheric Imaging Assembly (AIA) on the Solar Dynamics Observatory (SDO), Solar Phys., 275, 41-66, 2012.

Benkadda, S., Dudok de Wit, T., Verga, A., Sen, A, ASDEX Team, and Garbet, X.: Phys. Rev. Lett. 73, 3403, 1994.

Carbone, V., Lepreti, F., Primavera, L., Pietropaolo, E., Berrilli, F., Consolini, G., Alfonsi, G., Bavassano, B., Bruno, R., Vecchio, A., Veltri, P.: An analysis of the vertical photospheric velocity field as observed by THEMIS, A&A, 381, 265-270, 2002.

del-Castillo-Negrete, D., Hirshman, S. P., Spong, D. A., D'Azevedo, E. F.: Compression of magnetohydrodynamic simulation data using singular value decomposition, J. Comput. Phys., 222, 265-286, 2007.

Dudok de Wit, T., Moussauoi, S., Guennou, C., Auchere, F., Cessateur, G, Kretschmar, M., Vieira, L.A., Goriaev, F.F., Coronal Temperature Maps from Solar EUV Images: A Blind Source Separation Approach, Solar Phys. 283, 31–47, 2013.

Eckart, C., Young, G.: The approximation of a matrix by another of lower rank, Psychometrika, 1, 211-218, 1936.

Farge, M. and Schneider, K.: Wavelet transforms and their applications to MHD and plasma turbulence: a review, Journal of Plasma Physics, 81, 435810602, 2015.

Futatani, S., Benkadda, S., del-Castillo-Negrete, D.: Spatiotemporal multiscaling analysis of impurity transport in plasma turbulence using proper orthogonal decomposition, Phys. Plasmas, 16, 042506, doi:10.1063/1.3095865, 2009.

Futatani, S., Bos, W.J.T., del-Castillo-Negrete, D., Schneider K. , S. Benkadda, M. Farge: Coherent Vorticity Extraction in Resistive Drift-wave Turbulence: Comparison of Orthogonal Wavelets versus Proper Orthogonal Decomposition. Comptes Rendus Physique, 12, 2, 123-131, 2011.

Gallagher, P.T., Long, D.M., Large-scale bright fronts in the solar corona: a review of *EIT waves*, Space Science Rev., 158, 365–396, 2011.

Golub, G. H., van Loan, C. F. *Matrix Computations*. 3rd edition, John Hopkins, 1996.

Guennou, C., Auchere, F., Soubrie, E., Bocchialini, K., Parenti, S., Barbey, N., On the accurancy of the Differential Emission Measure Diagnostics of Solar Plasmas. Application to SDO/AIA II. Multithermal Plasmas, Astrophys. J. Supplement Series 203:25 1-13, 2012.

Hatch D. R. , Terry P. W., Jenko F. , Merz F., and Nevins W. M.: Saturation of Gyrokinetic Turbulence through Damped Eigenmodes. Phys. Rev. Lett. 106, 115003, 2011.

Holmes, P., Lumley, J., Berkooz, G.: Turbulence, Coherent Structures, Dynamical Systems and Symmetry, Cambridge University Press, Cambridge, UK, 1996.

Lawrence, J.K., Cadavid, A.C., Ruzmaikin, A.: Principal Component Analysis of the Solar Magnetic Field I: The Axisymmetric Field at the Photosphere, Solar Phys. 225:1-19, 2005.

Lemen, J.R., Title, A.M., Akin, D.J., Boerner, P.F., Chou, C., Drake, J.F., Duncan, D.W., Edwards, C.G., Friedlaender, F.M., Heyman, G.F., Hurlburt, N.E., Katz, N.L., Kushner, G.D., Levay, M., Lind- gren, R.W., Mathur, D.P., McFeaters, E.L., Mitchell, S., Rehse, R.A., Schrijver, C.J., Springer, L.A., Stern, R.A., Tarbell, T.D., Wuelser, J.-P., Wolfson, C.J., Yanari, C.: The Atmospheric Imaging Assembly (AIA) on the Solar Dynamics Observatory (SDO), Solar Phys., 275, 17-40, 2012.

Liu, R., Liu, C, Xu, Y., Liu, W., Kliem, B., Wang, H.: Observation of a Moreton wave and wave-filament interactions associated with the renowned X9 flare on 1990 May 24, Astrophys. J., 773:166, 1-13, 2013.

Martin, C. D., Porter, M. A.: The extraordinary SVD, e-print arXiv:1103.2338v5, 1-20, 2012.

Mininni, P. D.., Gomez, D. O., Mindlin, G. B.: Bi-Orthogonal Decomposition BOD of magnetic fields from magnetograms, Phys. Rev. Lett. 89, 061101, 2002.

Mininni, P. D., Lopez Fuentes, M., Mandrini, C. H., Gomez, D. O.: Study of Bi-Orthogonal modes in magnetic butterflies, Solar Phys., 219, 367-378, 2004.

Narukage, N., Eto, S., Kadota, M., Kitai, R., Kurokawa, H., Shibata, K.: *Proc. IAU Symposium* 223, 367-370, Stepanov, Benevolenskaya, Kosovichev (eds.), 2004

Podladchikova, O., Dudok de Wit, T., Krasnoselskikh, V., Lefebvre, B.: Quiet Sun Coronal heating: Analyzing large scale magnetic structures driven by different small-scale structures uniform sources, A&A 382, 713-721, 2002.

Rosenfeld, A., Kak, A.: Digital Picture Processing, Academic Press, New York, 1982.

Vecchio, A., Carbone, V., Lepreti, F., Primavera, L., Sorriso-Valvo, L., Veltri, P., Alfonsi, G., Straus, T.: Proper orthogonal decomposition of solar photospheric motions, Phys. Rev. Lett., 95, 061102, 2005.

Vecchio, A., Carbone, V., Lepreti, F., Primavera, L., Sorriso-Valvo, L., Straus, T, Veltri, P.: Spatio-temporal analysis of photospheric turbulent velocity fields using the proper orthogonal decomposition, Solar Phys., 251, 163-178, 2008.

Vecchio, A., Carbone, V.: Spatio-temporal analysis of solar activity: main periodicities and period length variations, Astron. & Astrophys., 502, 981-987, 2009.